The Astronomical Journal, 166:154 (11pp), 2023 October https://doi.org/10.3847/1538-3881/acf2f3

M67 Blue Stragglers with High-resolution Infrared Spectroscopy

K. E. Brady[1], C. Sneden[2], C. A. Pilachowski[1], Melike Afşar[2,3], G. N. Mace[2], D. T. Jaffe[2], N. M. Gosnell[4], and R. Seifert[2]
[1] Department of Astronomy, Indiana University, Bloomington, IN, USA
[2] Department of Astronomy and McDonald Observatory, University of Texas, Austin, TX, USA
[3] Department of Astronomy and Space Sciences, Ege University, İzmir, Turkey
[4] Department of Physics, Colorado College, Colorado Springs, CO, USA
Received 2023 February 23; revised 2023 August 15; accepted 2023 August 15; published 2023 September 12

Abstract

We report on the first detailed infrared chemical analysis of five binary members (S277, S997, S975, S1031, and S1195) in the open cluster M67 (NGC 2682). These stars are located outside (bluer and/or brighter than) the main-sequence turnoff region in M67. High-resolution ($R \sim 45{,}000$) near-infrared spectra were obtained with the Immersion GRating INfrared Spectrograph (IGRINS) at the McDonald Observatory 2.7 m Harlan J. Smith Telescope, providing full spectral coverage of the *H* and *K* bands. The abundances of C, Na, Mg, Al, Si, S, Ca, Fe, and Ni are measured using neutral atomic absorption lines. We detect $v \sin i \geqslant 25$ km s^{-1} in three of our program stars: S1031, S975, and S1195. We find our derived abundances to be in good agreement with turnoff star abundances, similar to published analyses of blue straggler stars in M67 from optical spectra. Detection of a carbon enhancement or depletion resulting from mass transfer is difficult due to the uncertainties in the carbon abundance and the relatively modest changes that may occur through red giant and asymptotic giant branch evolution.

Unified Astronomy Thesaurus concepts: Blue straggler stars (168); Open star clusters (1160); Stellar abundances (1577)

Supporting material: machine-readable table

1. Introduction

Blue straggler stars (BSSs) are classified as stars more luminous and/or bluer than the main-sequence (MS) cluster turnoff. These enigmatic stars appear as an extension of the MS on an optical color–magnitude diagram (CMD), seemingly lagging behind the standard stellar evolutionary track. Since their first detection in the globular cluster M3 (Sandage 1953), BSSs have been identified in other environments including open clusters (e.g., Milone & Latham 1994; Ahumada & Lapasset 2007), the Galactic field (e.g., Preston & Sneden 2000), and dwarf spheroidal galaxies (e.g., Momany et al. 2007). Now BSSs are accepted as components of all old stellar populations.

A variety of scenarios have been invoked to account for the origin of these late bloomers. Current theories for BSS formation focus on binary- and triple-star processes and include: (i) mass transfer through Roche-lobe overflow in binary systems (McCrea 1964); (ii) stellar collisions during dynamical encounters (Hills & Day 1976; Leigh & Sills 2011; Geller et al. 2013); and (iii) mergers of inner binaries in hierarchical triples driven by the Kozai mechanism (Perets & Fabrycky 2009; Naoz & Fabrycky 2014). Each formation mechanism is most likely responsible for a portion of the BSS population, though the distributions remain unknown (Stryker 1993; Leonard 1996). Furthermore, the dominant formation pathway may depend on the environment. In less-dense environments, such as open clusters and in the field, collisions of single stars are less likely than in high-density environments (Stryker 1993).

High-resolution infrared (IR) spectroscopy of the anomalous stars in clusters may provide additional evidence to constrain their formation, from the direct detection of cool, low-mass companions or by the derivation of evolutionary-sensitive elements of the CNO group. A particular advantage of IR spectra of binary stars is that the spectra are less likely to be altered by flux from hot companions.

Analyzing the surface compositions of BSSs may give insight on how they were formed. If formation occurs through mass transfer, the material gained may come from the stellar interior of the donor where abundances have been modified by CNO-cycle fusion. Depending on the type of mass transfer, normal carbon, nitrogen, and oxygen abundances or modest depletions or enhancements of these elements can be expected (Sarna & De Greve 1996). When mass transfer occurs while the donor is on the MS it is classified as Case A, after H exhaustion but before core ignition of helium as Case B, and after the ignition of helium as Case C (Kippenhahn & Weigert 1967; Lauterborn 1970). Conversely, if a blue straggler forms through a dynamical collision of two stars which results in a merger, minimal mixing occurs (Lombardi et al. 1995). Lombardi et al. (2002) indicates that the surface material from a merger comes from the more massive star.

The old (~4 Gyr), solar metallicity open cluster M67 (NGC 2682) is close in proximity (0.85 ± 0.04 Kpc; Angelo et al. 2019) and contains a significant population of BSSs (Geller et al. 2015; hereafter G15). Most BSSs are found to be binaries: G15 detected a binary frequency of $79\% \pm 24\%$ among the M67 blue stragglers. This cluster's blue straggler candidates, such as the 24 stars from Deng et al. (1999), have been studied extensively through photometric (e.g., Gilliland et al. 1991; Stassun et al. 2002; Sandquist & Shetrone 2003; Pandey et al. 2021), spectroscopic (e.g., Mathys 1991; Latham & Milone 1996; Shetrone & Sandquist 2000; Liu et al. 2008;

Bertelli Motta et al. 2018), and theoretical (e.g., Hurley et al. 2001, 2005) investigations.

Few of M67's blue stragglers, however, have been analyzed chemically. Previous M67 BSS abundance analyses include those of Mathys (1991), Shetrone & Sandquist (2000), and Bertelli Motta et al. (2018), in which 11 BSSs in total were analyzed. These chemical analyses all found the blue straggler surface abundances to be consistent with those of turnoff stars, which is indicative of a collisional formation mechanism (Lombardi et al. 1995).

We have gathered high-resolution near-infrared spectra of five binary members of M67 located blueward of and/or more luminous than the MS turnoff, with Sanders (1977)'s identifications of S277, S997, S1031, S975, and S1195. Section 2 describes the target selection, a literature review of our targets, observations, and data reduction. Section 3 details the line list construction, atmospheric parameter derivation, abundance analysis, non–local thermodynamic equilibrium (NLTE) corrections, and results. In Section 4, we discuss the rotational velocity of our program stars and put into context what our chemical composition results could mean for the stars' formation. In Section 5, we summarize the main conclusions from our study.

2. Observations and Data Reduction

2.1. Star Selection and Photometry

The program stars were selected from G15's M67 cluster membership study. G15 presented radial-velocity (RV) measurements for 1278 candidate members of M67 and computed membership probabilities for stars with $\geqslant 3$ RV observations. They sorted the candidate members into eight qualitative membership classes: single members/nonmembers, binary members/nonmembers, binary likely members, binaries with unknown RV membership, binary likely nonmembers, and unknown RV membership (see Table 3 in G15 for the selection criteria for each class). Binaries were identified by having an e/i statistic $\geqslant 3$, or having a binary orbital solution. The e/i statistic is the ratio of the standard deviation (e) to the expected precision (i) of the RVs for a given star. Stars with an $e/i < 3$ and without a derived binary orbital solution were classified as single stars, though G15 note that a number of these stars may be in long-period binaries.

Figure 1 shows a CMD with the designated single members, binary members, and binary likely members from G15 with Gaia Data Release 2 (DR2) photometry (Gaia Collaboration et al. 2018). Membership probabilities are from Gao (2018), with the exception of S277, S997, and S975, where the membership probabilities are from G15. To calculate membership probabilities, Gao (2018) used a machine-learning method, random forest (RF), based on astrometry and photometry taken from Gaia DR2. Table 1 displays the program stars, spectral types, equatorial coordinates, and basic photometry from G15.

IR photometry can provide further information on BSS binaries, as the type of companion to a blue straggler influences the location of the system on CMDs of different wavelengths. Hot companions may distort colors in an optical CMD, but will have less effect on an IR one. Figure 2 shows a K versus $J-K$ CMD of M67, using the IR photometry from the Two Micron All Sky Survey (2MASS) All Sky Catalog of point sources (Cutri et al. 2003). All of our program stars remain in positions more luminous and/or bluer than the MS, except for S1031,

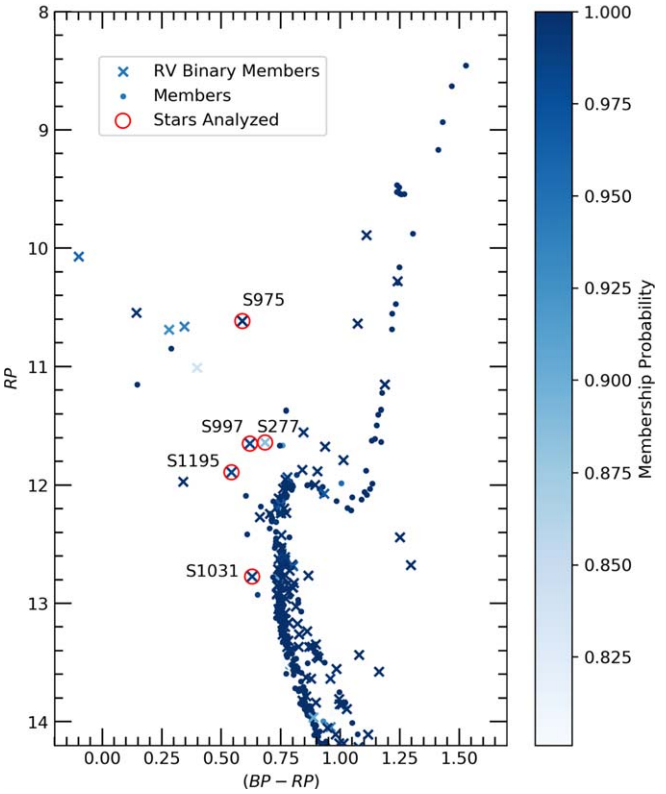

Figure 1. Optical CMD of M67 with designated members by G15 and photometry from Gaia DR2. RF cluster membership probabilities from Gao (2018) are indicated with the symbol shade of blue as defined by the color palate, with the exception of S277, S997, and S975, whose RV membership probabilities are from G15. The program stars are circled.

which appears on the MS in the K versus $J-K$ diagram. Its position in an optical CMD is likely due to the contribution of its white dwarf companion (see Section 2.2).

2.2. Descriptions of the Stars to Be Analyzed

Many of M67's blue stragglers have been analyzed previously; below we review what is known about the five binary systems in our sample.

S277 (WOCS 2068) is identified as a single-lined binary member (G15) of spectral type F6 V (Pickles 1998). G15 found S277's RV membership probability to be 84%, while Sanders (1977) found S277's proper-motion membership probability to be 93%. S277 was not included in Gao (2018)'s RF membership probability study. This star was included in the Deng et al. (1999) M67 BSS sample of 24 blue stragglers and is a long-period (8567 days), highly eccentric ($e = 0.859$) member with a binary mass function of 0.0681 (Leiner et al. 2019). G15 noted that S277 is located above the turnoff, but lies in an area that is expected to be populated by binaries containing normal MS turnoff stars. For this reason, S277 was excluded from the blue straggler sample in G15. S277 was included in Leiner et al. (2019)'s list of blue lurkers in M67, described by Leiner et al. (2019) to be lower-luminosity counterparts to the BSSs and identified by their anomalous rapid rotation given their age.

Leiner et al. (2019) found the ultraviolet (UV) flux of S277 was described best by two stars: one starting to turn off the MS, and one a blue straggler with a temperature of ~6800 K. They suggested that the system had been through a stellar dynamical

Table 1
Basic Stellar Properties of Our Sample of Binaries

Sanders No.[a]	WOCS ID	Spec. Type	R.A. (2000)	Decl. (2000)	V[b]	$(B-V)$[b]	PRV[c]	PPM	P (days)	e	UV Detection
S277	2068	F6 V	8:49:21.48	12:04:22.8	12.19	0.55	84	93[d]	8567[f]	0.859[f]	BSS+MSTO
S997	5005	F5 IV	8:51:19.90	11:47:00.4	12.13	0.46	98	99[e]	4913[g]	0.342[g]	BSS+WD
S1031	3001	F7 V	8:51:22.96	11:49:13.1	13.26	0.46	98	99[e]	128.14[f]	0.04[f]	BSS+WD
S975	3010	F5 V	8:51:14.36	11:45:00.5	11.08	0.43	98	90[d]	1221[g]	0.088[g]	BSS+WD?
S1195	1025	F2 V	8:51:37.69	11:37:03.8	12.28	0.38	94	99[e]	1154[g]	0.066[g]	BSS+WD?

Notes.
[a] Sanders identification number from Sanders (1977).
[b] V-band magnitude and $(B-V)$ index from G15 and references therein.
[c] RV membership probability from G15.
[d] Proper-motion membership probability from Sanders (1977).
[e] Proper-motion membership probability from Girard et al. (1989).
[f] Period, eccentricity, and UV detection from Leiner et al. (2019).
[g] Period and eccentricity from Latham & Milone (1996).

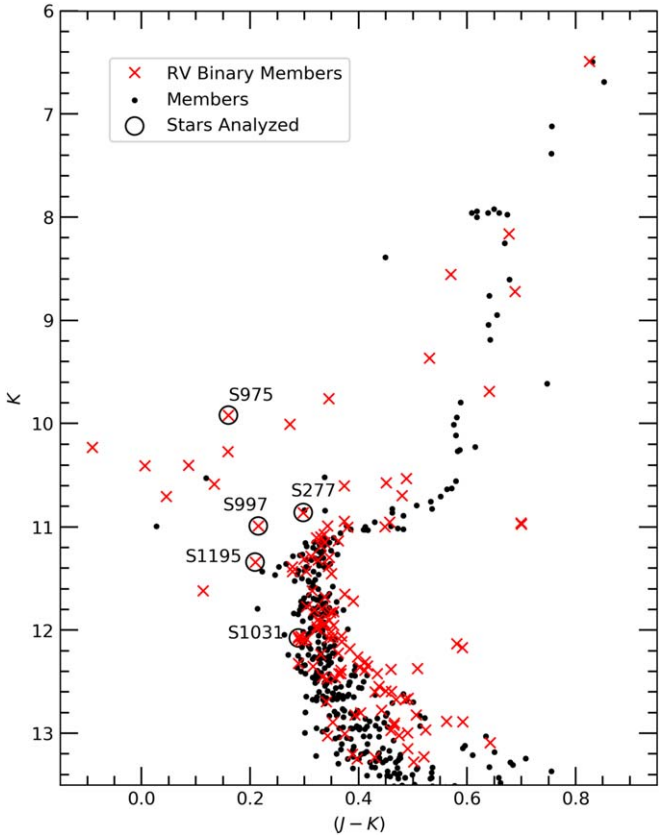

Figure 2. IR CMD of M67 with designated members from G15 and photometry from 2MASS (Cutri et al. 2003). The program stars are circled.

encounter that resulted in the collision of two MS stars, or a merger in a triple system. Leiner et al. (2019) found no evidence of a white dwarf in this binary system, and noted that it is unlikely for a white dwarf to have been ejected. Nine et al. (2023) found an indication of an MS stellar companion in the spectral energy distribution (SED) of S277 from their Hubble Space Telescope (HST) far-ultraviolet (FUV) survey of M67 blue lurkers. A mass function too large to correspond with a white dwarf companion was reported. The composition of this star has not previously been analyzed.

S997 (WOCS 5005) is a single-lined, long-period binary of 4913 days with high eccentricity ($e = 0.342 \pm 0.082$; Latham & Milone 1996). This F5 IV star (Allen & Strom 1995) is classified as a blue straggler by both G15 and Deng et al. (1999). The RV membership probability is 98% and the proper-motion membership probability is 99% (G15; Girard et al. 1989). S997 was not included in Gao (2018)'s RF membership probability study. Formation via mass transfer in a binary system is most likely ruled out due to the high eccentricity of the system (Latham & Milone 1996; Shetrone & Sandquist 2000). The blue straggler is the primary in this system, leaving a binary merger doubtful; this system would have to capture a star tidally after a merger, or be a triple system (Leonard 1996; Shetrone & Sandquist 2000).

van den Berg et al. (2004) found S997 to be an X-ray source from Chandra observations and speculated that a close binary may be responsible for the X-rays. S997 was also observed to be UV-bright from Galaxy Evolution Explorer observations of M67 (Sindhu et al. 2018). Pandey et al. (2021) detected a hot companion to this blue straggler using FUV photometry obtained with the Ultra Violet Imaging Telescope (UVIT) on AstroSat. Using white dwarf models, they categorized this hot companion to be a white dwarf with $T_{\rm eff} = 13{,}000 \pm 125$, $\log(g) = 7.75$, $L/L_{\odot} = 0.032 \pm 0.006$, and $R/R_{\odot} = 0.035 \pm 0.003$. Additionally, S997 was observed with the Space Telescope Imaging Spectrograph on the HST at low spectral resolution (Pandey et al. 2021). The Mg II h and k lines, which are known as excellent probes of the upper chromosphere (e.g., Leenaarts et al. 2013), were inspected in the HST spectrum of S997. These lines were found in absorption, indicating the absence of or low chromospheric activity (Sindhu et al. 2018; Pandey et al. 2021). The presence of Mg II h and k emission lines would have suggested significant chromospheric activity (Sindhu et al. 2018). The HST spectra gave additional evidence of FUV excess and confirmation of the presence of both a cool and a hot component in the system (Pandey et al. 2021). S997 has been previously chemically analyzed by Shetrone & Sandquist (2000), who suggested S997 may be a collision product after detecting C and O abundances comparable to turnoff stars.

S1031 (WOCS 3001) lies on the blue side of the MS turnoff and SIMBAD[5] indicates a spectral type of F7 V. Despite its blue location, this star was not included in the Deng et al. (1999) or G15 candidate BSS lists. G15 left S1031 out from

[5] http://simbad.u-strasbg.fr/simbad/

their sample due to its proximity to the blue hook region on a CMD, so it could not be confidently classified as one of M67's blue stragglers (G15; Leiner et al. 2019). S1031 was included in Leiner et al. (2019)'s list of M67 blue lurkers. G15 classified S1031 as a single-lined binary with an RV membership probability of 98%. Girard et al. (1989) estimated its proper-motion membership probability to be 99%. S1031 was included in Gao (2018)'s RF cluster membership study, who found the membership probability to be 99.3%.

Jadhav et al. (2019) observed this binary system using the UVIT and suggested the observed excess of UV flux was the result of a white dwarf companion of 12,500 K and 0.3–0.45 $M_{\odot}$. They noted that while the 0.3−0.45 $M_{\odot}$ white dwarf may or may not require mass transfer, the circularized orbit and rapid rotation are indicative of mass transfer in close binaries. Leiner et al. (2019) found $v \sin i = 14.7$ km s^{-1}, $P = 128.14$ days, $e = 0.04$, and a binary mass function = 0.0143. Leiner et al. (2019) noted that the orbital period of just a few hundred days suggests this system could be the result of Case B mass transfer from a red giant branch (RGB) donor. The detection of S1031's high rotation rate gives further evidence of its relation to the blue stragglers (Leiner et al. 2019). Nine et al. (2023) reported evidence for a 10,300–10,500 K white dwarf companion of 0.36–0.43 $M_{\odot}$ to S1031 from their HST UV observations. Their best-fit temperatures corresponded to a cooling age of ∼600–900 Myr. Based on the orbital properties of the system, Nine et al. (2023) suggested the companion is an He white dwarf that is the result of Case B mass transfer, though FUV spectroscopy is needed for confirmation. This star has not previously been analyzed for composition.

S975 (**WOCS 3010**) is a single-lined binary star (G15) of spectral type F5 V (Pickles 1998) with rapid rotation ($v \sin i = 50$ km s^{-1}; Latham & Milone 1996). Both Deng et al. (1999) and G15 include S975 in their BSS samples. S975's proper-motion membership probability is 90% and its RV membership probability is 98% (Sanders 1977; G15). S975 was not included in Gao (2018)'s RF membership probability study.

This star was previously chemically analyzed by Shetrone & Sandquist (2000) who measured a $v \sin i$ of 48 km s^{-1}. They suggested this was a mass-transfer system as their measured O abundance was high in comparison to turnoff stars, but noted the system appeared to have a companion that affected the line flux. S975's orbital solution was calculated by Latham & Milone (1996), who found the period to be 1221 days and the eccentricity to be small ($e = 0.088 \pm 0.060$). The long period and small eccentricity may be an indication of a past interaction. Preston & Sneden (2000) suggested the blue stragglers in their blue metal-poor star sample were formed by mass transfer, as they had long periods and small orbital eccentricities characteristic of McClure carbon star binaries (see the bottom panel of Figure 19 in Preston & Sneden 2000). The carbon star binaries of McClure (McClure & Woodsworth 1990; McClure 1997) exhibited long periods and low orbital eccentricities, which McClure explained by orbit dissipation occurring with mass transfer in the system. Leonard (1996) suggested the formation of S975 may be due to Case C (asymptotic giant branch, AGB) mass transfer. Landsman et al. (1998) reports strong evidence of a hot subluminous companion to S975 in their UV photometry. Landsman et al. (1998) suggests that the existence of a hot subluminous companion along with a nearly circular binary orbit indicates that the formation is due to a binary mass-transfer process. Sindhu (2019) detected a UV excess consistent with this subluminous, hot companion through SED fitting of S975. The hot component has a $T_{\rm eff} = 13{,}750$–$16{,}500$ K, $R/R_{\odot} = 0.047$–0.029, and mass ∼0.18 $M_{\odot}$, suggesting the companion is a white dwarf.

S1195 (**WOCS 1025**) is defined as a single-lined binary star (G15) of spectral type F2 V (Pickles 1998). This star was one of the 24 candidate BSSs from Deng et al. (1999) and included in the G15 blue straggler candidate sample. Girard et al. (1989) estimated its proper-motion membership probability to be 99% while G15 estimated its RV membership to be 94%. Gao (2018) found S1195's RF membership probability to be 99%. Latham & Milone (1996) estimated the period to be 1154 days, the eccentricity to be 0.066 ± 0.082, and the $v \sin i$ to be 60 km s^{-1}. The circularized orbit paired with a large $v \sin i$ suggests recent mass-transfer episodes for this single-lined binary (Pandey et al. 2021).

When observing this system, Pandey et al. (2021) detected a UV excess and reported that this blue straggler likely has a hot companion with a $T_{\rm eff}$ in the range 21,000–50,000 K, but more data in the UV are needed to estimate its parameters confidently. This star has not previously been analyzed for composition.

2.3. IGRINS Spectra

Spectroscopic observations of the five stars were carried out with the high-resolution H and K photometric band Immersion GRating INfrared Spectrograph (IGRINS; Yuk et al. 2010; Park et al. 2014; Mace et al. 2016)[6] at the McDonald Observatory 2.7 m Harlan J. Smith Telescope. Target acquisition was straightforward and there was no source confusion in the field of any target.

A single IGRINS observation delivers full spectral coverage of the H (∼1.5−1.7 μm) and K (∼2.0−2.4 μm) bands with resolving power $R \equiv \lambda/\Delta\lambda \simeq 45{,}000$. Each BSS target observation was accompanied by observation of a hot, mostly featureless star usually of spectral type A0V to be used in the removal of telluric lines.

Each complete observation of a target star consisted of 1−2 sets of four individual integrations taken in an A-B-B-A pattern, where A and B integrations were accomplished with the target shifted on the slit perpendicular to the dispersion direction by 7″. The exposure time for each integration was 600 s, resulting in total exposure times of 4800 s (80 minutes) for all BSS stars except S975, for which only one set of four integrations was accomplished. Exposure times for the hot-star observations varied but were always adequate to attain a good signal-to-noise ratio (S/N) in the reduced spectra.

The IGRINS Pipeline Package[7] was used to reduce the data (Lee & Gullikson 1970). The pipeline performs flat fielding, background removal, order extraction, distortion correction, wavelength calibration, and telluric removal. To normalize the data, each spectrum was divided by a cubic spline fit to the continuum. Figure 3 shows a spectral region from 15970–16065 Å for our five targets.

3. Analysis and Results

In this section we detail our line list construction, calculation of atmospheric parameters, and abundance measurement methods. The results of our abundance analysis are presented

[6] http://www.as.utexas.edu/astronomy/research/people/jaffe/igrins.html
[7] https://github.com/igrins/plp

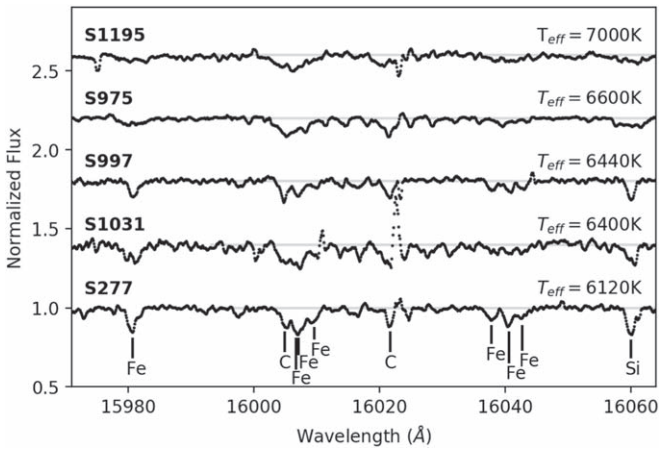

Figure 3. A sample spectral region in the *H* band. The spectra are arranged in order of decreasing $T_{\rm eff}$ from top to bottom. Rotational broadening of the spectral lines can be seen in S1031, S975, and S1195. The derived rotational velocities are shown in Table 3.

and compared to results from previous chemical studies. The reliability of the measured spectral lines is evaluated in terms of departures from LTE.

3.1. Line List

Atomic line data for the spectral lines come from Afşar et al. (2018) and the atomic and molecular line list generator *linemake* (Placco et al. 2021). The log(*gf*) values were calibrated two ways, first by fitting a high-resolution solar spectrum with a synthetic spectrum and, second, by adjusting MOOG's equivalent width line analysis (Sneden 1973) to produce solar abundances. Solar abundances were adopted from Asplund et al. (2009). The averages of the resulting log (*gf*) values from the two procedures were taken to be the final log(*gf*) values for the lines. Table 2 shows the final line list adopted.

We note that the lines of C I arise from high excitation levels and are likely formed in NLTE (Fabbian et al. 2006). By using log(*gf*) values derived from fitting these lines in the solar spectrum to obtain the known solar [C/H] abundance with an LTE model, we are implicitly including an approximate NLTE correction at the solar effective temperature.

3.2. Effective Temperatures

We calculated the photometric temperatures of the stars using the $T_{\rm eff}$ and color relation from González Hernández & Bonifacio (2009):

$$\theta_{\rm eff} = b_0 + b_1 X + b_2 X^2 + b_3 X[{\rm Fe/H}] + b_4[{\rm Fe/H}] + b_5[{\rm Fe/H}]^2, \quad (1)$$

where $\theta_{\rm eff} = 5040/T_{\rm eff}$, X is the color, and b_i ($i = 0,\ldots,5$) are the coefficients of the fit. The effective temperature for each star was calculated four times using $E(B-V)$ from Bellini et al. (2010) and the stars' $B-V$, $V-J$, $V-H$, and $V-K$ colors. The b_i coefficients for dwarf stars were used. The final effective temperatures are the averages of the four photometric temperatures for each star. These effective temperatures and their standard deviations are shown in Table 3. Two of our program stars, S975 and S1195, show much larger differences between the $B-V$ temperature and the $V-J$, $V-H$, and $V-K$ temperatures. The differences between the $B-V$ temperature and the average of the $V-J$, $V-H$, and $V-K$ temperatures were ~1040 K and ~680 K, respectively. Due to this dispersion in the effective temperatures from the four colors, we used an average of the effective temperatures from Liu et al. (2008) and references therein for S975 and S1195. The effective temperatures from Liu et al. (2008) are consistent with the calculated $V-J$, $V-H$, and $V-K$ temperatures. Liu et al. (2008) also gives effective temperatures for S277 and S997, which are consistent with the effective temperatures adopted in our study.

Table 2
Line List

Element	$\lambda_{\rm vacuum}$ (Å)	χ (eV)	log(*gf*)	Source[a]
C I	16004.9	9.624	0.18	2
C I	16021.7	9.63	0.15	1
C I	16890.386	9	0.355	1
C I	17234.473	9.69	0.113	2
C I	17274.945	9.688	0.325	2
C I	21023.131	9.17	−0.44	1
C I	21191.345	9.827	−0.25	2
C I	21191.839	9.827	−0.48	2
C I	21259.256	9.826	−0.8	2
C I	21259.934	9.826	0.3	2
…				

Note.
[a] Sources for the excitation potential values: (1) Afşar et al. (2018); (2) Placco et al. (2021).

(This table is available in its entirety in machine-readable form.)

Table 3
Derived Stellar Properties

Sanders No.	WOCS ID	$T_{\rm eff}$ (K)	log *g*	ξ (km s^{-1})	*v* sin *i* (km s^{-1})
S277	2068	6120 ± 121	3.6	2.7	<14
S997	5005	6440 ± 48	3.6	1.8	<20
S1031	3001	6400 ± 34	4.1	1.3	25 ± 6
S975	3010	6600[a]	4.1[a]	1.6	51 ± 5
S1195	1025	7000[a]	4.5[a]	2.3	58 ± 6

Note.
[a] Values from Liu et al. (2008) and references therein.

3.3. Surface Gravities

The standard equation for physical gravities depends on mass:

$$\log\ g_\star = 0.4(M_{V\star} + BC - M_{\rm Bol\odot}) + \log\ g_\odot + 4\log\left(\frac{T_{{\rm eff}\star}}{T_{{\rm eff}\odot}}\right) + \log\left(\frac{m_\star}{m_\odot}\right). \quad (2)$$

Previous studies of BSSs in open clusters have found them to be a few tenths of a solar mass greater than the cluster's turnoff mass. For example, Jadhav et al. (2021) found BSS masses between 1.2−1.9 $M_\odot$ in the old open cluster King 2. Sandquist et al. (2021) determined a turnoff mass of 1.22 $M_\odot$ for M67, and a mass of 1.32 $M_\odot$ for the bluest subgiants in the cluster.

Stello et al. (2016) found masses of 1.36 $M_{\odot}$ for M67 giants from asteroseismology.

Since the masses of our specific targets are uncertain, we adopted the surface gravities from Liu et al. (2008) for S975 and S1195. When the surface gravities for S975 and S1195 are computed using Equation (2), log g is equal to 3.13 and 3.85, respectively. S1031 lies near the MS, slightly below the turnoff, and we adopted a mass of 1.1 $M_{\odot}$ for a surface gravity of log $g = 4.1$. S997 and S277 both lie about half a magnitude above the early subgiant sequence, and redward of the extension of the MS. For these stars we adopted surface gravities log $g = 3.6$, consistent with the possible mass ranges and their evolutionary state. We note that the sensitivity of our derived abundances to a change in surface gravity of $\Delta\log\ g = +0.3$ is typically -0.01 or -0.02 dex in Fe in abundance. Neither the adopted stellar mass nor the surface gravity has a significant effect on our results. The adopted surface gravity for each star is included in Table 3.

3.4. Microturbulent Velocities

For two of the stars in our sample, S277 and S997, the spectra allowed for a detailed equivalent width analysis as the line profiles were not rotationally broadened. For these stars, the microturbulence was derived from abundance versus line strength plots for the measured Fe lines, using the adopted effective temperature and surface gravity. For the remaining stars S1031, S975, and S1195 with spectra that were more blended, microturbulent velocities were calculated using the relation from Gebran et al. (2014):

$$\xi_t = 3.31 \times \exp\left[-\left(\log\left(\frac{T_{\rm eff}}{8071.03}\right)^2 \Big/ 0.01045\right)\right], \quad (3)$$

which applies to our sample of F-type stars. This relation gives microturbulent velocities of 0.83 km s^{-1} for S277 and 1.3 km s^{-1} for S997. Microturbulent velocities do not dominate the uncertainty of the derived abundances in the BSSs, so the differences in the derived microturbulent velocities from the two approaches do not have a significant impact. The final microturbulent velocities are shown in Table 3.

3.5. Assumed Metallicities

M67 has been studied at high spectral resolution many times and all studies agree that it has essentially solar metallicity. A sample of published values in recent years includes -0.03 ± 0.03 (Tautvaišiene et al. 2000), $+0.02 \pm 0.04$ (Yong et al. 2005), $+0.03 \pm 0.03$ (Randich et al. 2006), $+0.01 \pm 0.03$ (Santos et al. 2009), $+0.05 \pm 0.02$ (Pancino et al. 2010), -0.01 ± 0.05 (Jacobson et al. 2011), $+0.04 \pm 0.02$ (Hawkins et al. 2016), and $+0.03 \pm 0.05$ (Netopil et al. 2016). Therefore, we adopt [Fe/H] = +0.02 for this study, the average of the published values.

3.6. Abundance Fitting and Results

The analysis method for each spectral line was determined individually by the degree of blending of each profile. For blended lines, spectra were synthesized using the current version of the LTE, plane-parallel, spectral line analysis code MOOG along with MARCS 1D atmospheric models (Gustafsson et al. 2008). Synthetic spectra were generated using the derived atmospheric parameters and overplotted on the observed spectra. Fits were visually adjusted. For lines that were not blended, the equivalent widths were measured with the IRAF task *splot*. The abundances of each transition were derived by requiring the computed and measured equivalent widths to agree. The final elemental abundances of C, Na, Mg, Al, Si, S, Ca, Fe, and Ni are shown in Table 4. Column 1 is the observed element. Subsequent columns show the abundance [M/H] for each element. Solar log $\epsilon(A)$[8] values from Asplund et al. (2009) were used to determine the [M/H] values. The standard deviation along with the number of lines are also given. The final uncertainties were computed from the sum in quadrature of the individual uncertainties for the atmospheric parameters and observational uncertainties. The average surface abundances and standard deviations for the set of program stars are shown in the last two columns. Due to line weakening and/or smearing from the high temperature or rapid rotation of S1031, S975, and S1195, some of the elemental abundances could not be measured.

The surface abundances of the program stars are generally consistent with those of turnoff stars. Figure 4 shows the derived abundances for six of our elements as a function of effective temperature. Abundance measurements of turnoff stars in M67 from Shetrone & Sandquist (2000) and from APOGEE[9] spectra from Souto et al. (2019) are plotted for comparison. In particular, our iron abundance does not significantly differ from the cluster average. Our results for Al and Ca are consistent with the average values for turnoff stars. The measured Si and Mg abundances are slightly higher than turnoff star abundances, but are within the errors. Carbon abundances are discussed further in Section 3.7. APOGEE results for Mg, Si, and Al all suggest a strong temperature dependence, but our results do not.

Our results are similar to the previous M67 blue straggler optical chemical composition studies of Mathys (1991), Shetrone & Sandquist (2000), and Bertelli Motta et al. (2018), who also found the surface abundances of their BSSs to be in agreement with turnoff star abundances. The Shetrone & Sandquist (2000) and Bertelli Motta et al. (2018) BSS abundances are shown in Figure 4 for comparison.

Two stars in our sample, S997 and S975, were previously analyzed by Shetrone & Sandquist (2000). Their analysis was based on spectra covering from 3800 to 10100 Å. Shetrone & Sandquist (2000) photometrically determined their effective temperatures using the equation from Soderblom et al. (1993), then fine tuned the temperatures by forcing the slope of abundances from Fe I lines versus excitation potential to be zero. Their final effective temperatures are ∼200 K greater than our final effective temperatures. For S997 and S975, the sensitivity of our derived abundances to a change in temperature of ±100 K is less than 0.1 dex in abundance. The surface gravities and microturbulances for both S997 and S975 in Shetrone & Sandquist (2000) are also higher than our values. C, Mg, Ni, Na, and Ca abundances were measured in both of our studies. Within the precision of both studies, our surface abundance measurements agree with those of Shetrone & Sandquist (2000), with the exception of [C/H] in S975 and [Mg/H] and [Ca/H] in S997, which we find to be higher.

[8] We use the standard spectroscopic notation where log $\epsilon(A) \equiv \log(N_A/N_{\rm H}) + 12.0$ and $[A/B] \equiv \log(N_A/N_B)_{\rm star} - \log(N_A/N_B)_{\odot}$ for elements A and B.

[9] Apache Point Observatory Galactic Evolution Experiment: https://www.sdss.org/dr16/irspec/.

Table 4
Stellar Abundances

	S277			S997			S1031			S975			S1195				
Element	[M/H]	σ	n	[M/H]	σ	n	[M/H]	σ	n	[M/H]	σ	n	[M/H]	σ	n	Avg.	σ
C[a]	−0.22	0.08	10	−0.09	0.11	5	0.11	0.26	3	0.24	0.19	3	0.17	0.27	5	0.04	0.20
Na	0.24	0.14	1	0.00	0.17	1	…	…	…	…	…	…	…	…	…	0.12	0.16
Mg	0.05	0.12	1	0.30	0.12	2	0.08	0.26	2	−0.10	0.19	2	−0.10	0.23	2	0.05	0.19
Al	0.24	0.14	3	−0.09	0.13	2	0.17	0.23	2	−0.03	0.19	2	…	…	…	0.07	0.18
Si	0.06	0.16	11	0.22	0.11	9	0.35	0.23	8	0.13	0.18	3	0.00	0.24	3	0.15	0.19
S	0.15	0.13	2	0.03	0.14	2	0.05	0.28	1	0.27	0.20	2	…	…	…	0.13	0.20
Ca	0.10	0.09	7	0.31	0.14	6	−0.02	0.25	3	0.00	0.18	2	…	…	…	0.10	0.18
Fe	0.00	0.06	46	−0.01	0.10	46	0.01	0.23	23	−0.10	0.19	30	0.03	0.23	24	−0.01	0.18
Ni	−0.16	0.12	2	−0.10	0.18	2	0.30	0.27	2	…	…	…	…	…	…	0.01	0.20

Note. n = number of lines.
[a] Differentially corrected for NLTE using Fabbian et al. (2006)'s results.

Differences in the derived carbon abundances are discussed in Section 3.7.

3.7. C I Line Formation

The C I lines used to determine the abundance of carbon in the BSSs are all high-excitation lines with excitation potentials of 9 eV or above. Typical equivalent widths of the carbon lines are around $\log(\omega/\lambda) = -4.9$. Amarsi et al. (2019) investigated 3D NLTE departures from simple, LTE line formation for high-excitation C I lines in the solar photosphere, and found that corrections for near-infrared lines are typically 0.05 dex or less for the disk-integrated flux. While the NLTE corrections can be modest, neglecting neutral hydrogen impact excitation can create larger deviations from an LTE model (Amarsi et al. 2019). Tomkin et al. (1992) included an NLTE analysis of the the 9100 Å C I lines used in their abundance study of halo dwarfs. They found the NLTE corrections for the 7.48 eV C I lines to be on the order of 0.05 dex, but observed an effective temperature dependence in the C abundances. They noted the temperature dependence may be due to the representation of the NLTE effects, and specifically, the treatment of neutral hydrogen collisions. Fabbian et al. (2006) provided neutral carbon NLTE corrections for the ∼7.5 eV lines at approximately 9000 Å, and reported large, negative NLTE abundance corrections for high-excitation neutral carbon permitted lines.

As a simple check on the reliability of the C I lines used in our analysis, we selected four MS stars from the IGRINS spectral library (Park et al. 2018) covering a range of temperatures from $5801 \leqslant T_{\rm eff} \leqslant 6573$ K. The spectra, observed with the same instrument and resolution as our BSSs, have S/Ns typically $\geqslant$ 200. We derived [C/H] abundances using the atmospheric parameters adopted by Park et al. (2018) to identify any strong dependence of [C/Fe] on temperature that might indicate a departure from LTE. No dependence of [C/Fe] on temperature was found, though all of the stars are unexpectedly C rich. The derived [C/H] abundances are given in Table 5.

NLTE corrections were not applied to the ∼8.6 eV carbon lines in Shetrone & Sandquist (2000), and it is unclear what corrections might be appropriate for these carbon lines or the 9 + eV lines used in our study. In Ferraro et al. (2006)'s chemical analysis of BSSs in the globular cluster 47 Tuc, an NLTE correction was derived by interpolating the C I abundances from Tomkin et al. (1992) and applied to the 7.48 eV C I line at 9111.8 Å. The large corrections for the 7.5 eV lines from Fabbian et al. (2006) suggest significant NLTE corrections are likely, on the order of −0.2 to −0.4 dex, depending on the effective temperatures and surface gravities of our program stars.

We estimate neutral carbon NLTE corrections for our program stars with the Fabbian et al. (2006) results to provide differential corrections compared to the Sun. The $\log(gf)$ values in our line list were derived from comparison with the solar spectrum. Therefore, spectral analysis with these $\log(gf)$ values includes the solar correction for NLTE, resulting in an abundance that is partially corrected for NLTE. Differential corrections are then made with the Fabbian et al. (2006) results based on the temperature and gravity of the Sun and our program stars. When the Fabbian et al. (2006) corrections are applied to our BSS and IGRINS spectral library star carbon abundance measurements, the average carbon abundance in both groups is reduced by ∼0.1 dex. The final BSS carbon abundances that are differentially corrected for NLTE are shown in Table 4.

In comparison to our NLTE-corrected carbon abundances, the carbon abundance for S997 derived by Shetrone & Sandquist (2000) is the same, while for S975 our result is higher by ∼0.3 dex. We adopted Shetrone & Sandquist (2000) 's atmospheric parameters and repeated our carbon abundance analysis of our program stars. For S997, we find $[C/H] = 0.02 \pm 0.11$. This is slightly closer to the turnoff value for carbon compared to our $[C/H] = 0.08$ result where NLTE corrections from Fabbian et al. (2006) were not yet applied. Adopting the Shetrone & Sandquist (2000) model atmosphere parameters gave the same carbon abundance for S975: $[C/H] = 0.32 \pm 0.19$, the carbon abundance before differential NLTE corrections were applied.

Overall, the C I lines used in this study are new to abundance determinations, are sufficient in strength, and reside in spectral regions free from telluric lines. However, they may be sensitive to 3D and/or NLTE effects, which would result in too large LTE abundances. We estimate neutral carbon NLTE corrections for our program stars, but an NLTE analysis of these high-excitation lines is needed to understand their behavior better.

4. Discussion

4.1. Rotation Velocity

We measure rotational velocities ($v \sin i$) for three of our program stars: S975, S1031, and S1195. By fitting the rotational broadening of the spectral lines, we found $v \sin i = 25 \pm 6$ km s^{-1}

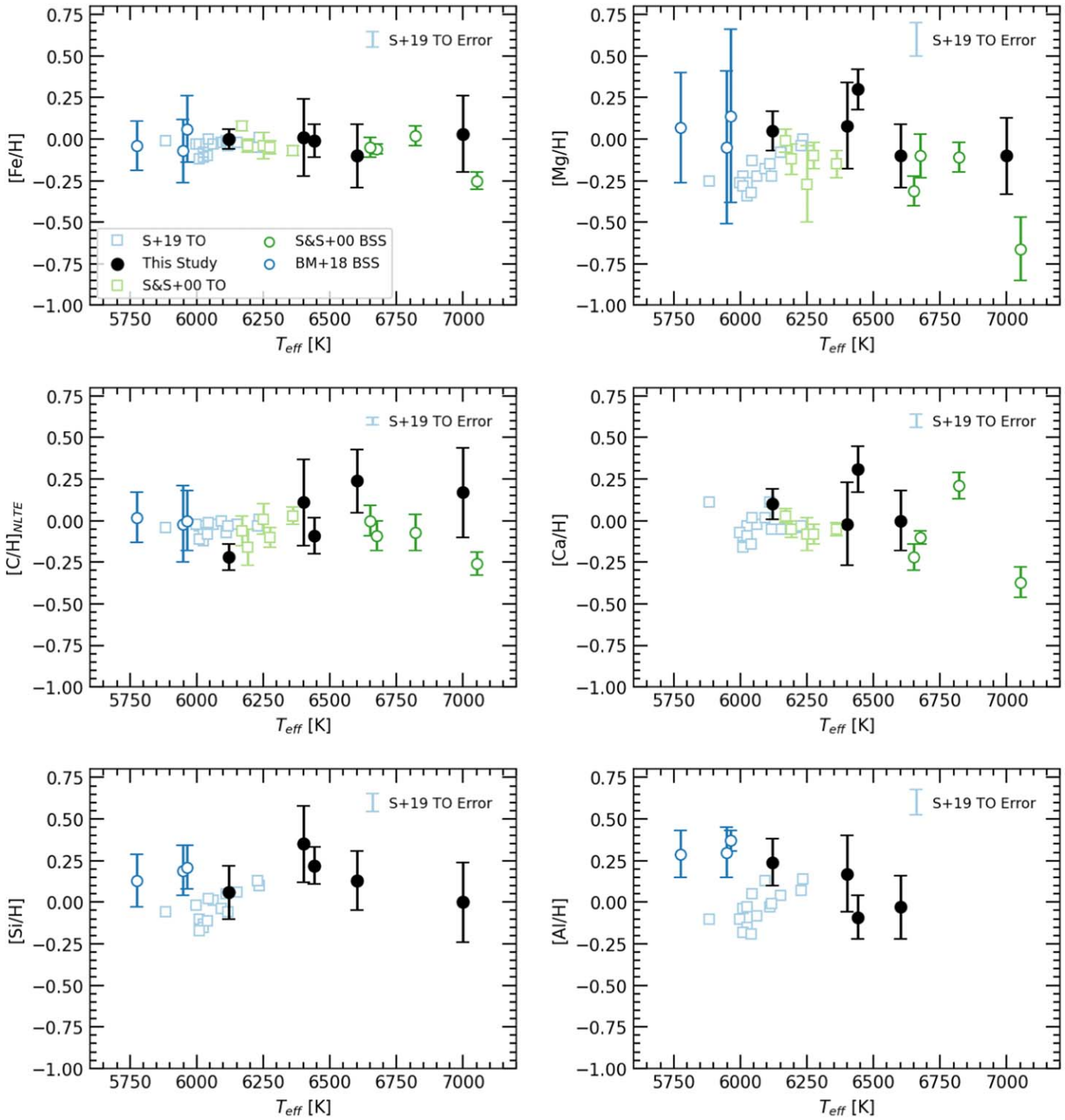

Figure 4. Chemical abundance vs. effective temperature. The BSSs from our analysis are shown as black circles. BSS error bars are one standard deviation. M67 turnoff star abundances from Souto et al. (2019) are shown as blue squares and from Shetrone & Sandquist (2000) as green squares. Uncertainties from Souto et al. (2019) are shown in the upper right corner of each panel. M67 BSS abundances from Bertelli Motta et al. (2018) are blue circles and from Shetrone & Sandquist (2000) are green circles. Data from the literature are unfilled symbols.

for S1031, $v \sin i = 51 \pm 5$ km s^{-1} for S975, and $v \sin i = 58 \pm 6$ km s^{-1} for S1195. The rotation detected is comparable to the v sin i values from Nine et al. (2023) and Leiner et al. (2019) for S1031 (24.7 km s^{-1}and 14.7 km s^{-1}, respectively), Shetrone & Sandquist (2000) for S975 (50 km s^{-1}), and Latham & Milone (1996) for S975 (50 km s^{-1}) and S1195 (60 km s^{-1}).

Rotation rates may evolve with time in mass-transfer objects. Spin-up of the mass-accreting star is expected from significant angular momentum transport during mass transfer (Packet 1981; de Mink et al. 2013; Matrozis et al. 2017). Likewise, stellar collisions and mergers can result in stars with rapid rotation (Sills et al. 2001, 2005). Leiner et al. (2018)

Table 5
IGRINS Spectral Library Star Abundances

Star	Spectral Type	$T_{\rm eff}$[a] (K)	[Fe/H][a]	log g[a]	[C/H]
HD71148	G1 V	5801	−0.04	4.36	0.31 ± 0.14
HD87141	F5 V	6359	0.09	3.90	0.18 ± 0.14
HD91752	F3 V	6418	−0.23	3.96	0.04 ± 0.14
HD87822	F4 V	6573	0.10	4.06	0.35 ± 0.14

Note.
[a] Stellar atmospheric parameters are from Park et al. (2018) and references therein.

recently conducted the first observational study of spin-down in post–mass-transfer binaries, where the stars spin-down as they age in a similar form that is predicted for standard solar-type stars. The gyro-age clock is reset and old stars can be seen with rapid rotation typical of younger stars (Leiner et al. 2018). Rapid rotation rates may be indicative of a recent stellar interaction (e.g., Leiner et al. 2019), which is relevant for three of our stars (S975, S1031, and S1195). Unfortunately, the v sin i values do not appear to give information on what formation mechanism occurred, as multiple interactions can lead to rapid rotation.

Subramaniam et al. (2020) found a moderate correlation between the temperature of a white dwarf companion and the v sin i of the blue straggler (see Figure 3 in Subramaniam et al. 2020). They concluded that BSSs with faster rotation have hot white dwarf companions, while slower rotating BSSs do not have hot companions. Together with the predicted temperatures of the white dwarf companions, our v sin i measurements support Subramaniam et al. (2020)'s conclusion that the white dwarf companions of fast-rotating blue stragglers and blue lurkers are hot.

4.2. Possible Blue Straggler Formation Histories

The derived surface abundances of the program stars are generally consistent with those of turnoff stars. This is in agreement with the previous M67 BSS abundance analyses of Mathys (1991), Shetrone & Sandquist (2000), and Bertelli Motta et al. (2018).

Each star in our sample could have a different history, and through the possible detection of a change in initial abundances, carbon has been considered to be an important indicator of what those histories might be. Given the complexity of carbon, we are unable to determine if carbon is enhanced or depleted with certainty, and a [C/Fe] similar to that of turnoff stars is most likely. We detect possible carbon enhancements for S975 and S1195 consistent with predicted AGB-phase mass transfers, possible carbon depletion in S277 inconsistent with the predicted stellar dynamical encounter or a merger in a triple system formation, no carbon enhancement or depletion in S997 which is inconsistent with the predicted mass-transfer formation mechanism, and no evidence of depletion of carbon in S1031 from the predicted RGB-phase mass transfer. Ultimately, we are hesitant to use carbon abundances as an indicator of mass transfer due to the large uncertainties associated with NLTE effects. With the inconclusive C abundances, determining the histories of the systems mainly relies on dynamical and white dwarf companion information. The expected range of carbon abundances from different formation scenarios is too small given the observational errors (Charbonnel & Lagarde 2010).

Comparing the location of the BSSs on the IR CMD versus the optical CMD may give insight into the formation mechanisms of the BSSs through detection of the companion's influence on the observed colors. The location of S277 on the IR CMD is comparable to its optical location, providing evidence in favor of a dynamical collision or merger in a triple system, as a white dwarf that would imply mass transfer is not detected. While S1031 lies blueward of the MS turnoff in the optical, it appears on the MS in the IR, suggesting a hot companion is contributing to the star's optical color. S975 remains in a position bluer and more luminous than the MS turnoff in the IR CMD, which can be explained by the subluminous nature of the white dwarf companion. The location of S997 in the IR CMD is comparable to its optical location, confirming the hot companion is faint in nature. No evidence of a hot companion to S1195 was found from the IR CMD. The locations of the BSSs in the IR CMD versus the optical CMD generally support the conclusions drawn from the SED analyses of the individual BSSs described in Section 2.2.

5. Summary and Conclusions

The first detailed IR chemical analysis of five binary members of the old open cluster M67 located above and/or blueward of the clusters MS turnoff is reported. We measured C, Na, Mg, Al, Si, S, Ca, Fe, and Ni abundances in the program stars using high-resolution, IR spectra covering the H and K bands. Our principal conclusions are as follows:

1. The detected compositions of the five anomalous stars in this study are generally consistent with those of turnoff stars in M67.
2. The abundances from our program stars determined from IR spectroscopy generally agree with the results obtained from optical spectroscopy.
3. The projected rotational velocities determined from the IR spectra generally agree with those from the optical spectra.
4. S1031 is displaced blueward from the MS in the RP versus $(BP - RP)$ but lies on the MS in the K versus $(J - K)$ diagram. Flux from a hot companion may be the cause of the displacement in the $(BP - RP)$ color.
5. Rapid rotation is detected in S1031, S975, and S1195, which together with the possible carbon enhancements of S975 and S1195 from the IR spectra and location of S1031 on an IR CMD, may be indicative of recent stellar mass transfer in a binary system.
6. The near-infrared, high-excitation neutral carbon lines of 9+ eV are used for the first time in stellar abundance determinations, and require further NLTE analysis to understand their behavior better.

Our spectroscopic analysis of these five binary members does not provide conclusive evidence of altered composition that would be indicative of certain formation mechanisms. The relative decreases of C on the RGB of mass transfer that occurs at that phase, are small and difficult to detect. Detection of the enhancements from post-AGB evolution will also be minimal and difficult to see due to the uncertainties in the C abundances. We are skeptical to use carbon abundances as an indicator of mass transfer due to the large uncertainties associated with NLTE effects and the relatively modest changes that may occur

through red giant and AGB evolution. The derived surface abundances are generally consistent with those of turnoff stars, and elemental abundances that vary significantly from the turnoff values need additional line measurements for definitive conclusion. These results agree with previous optical studies of M67 BSS chemical compositions.

Acknowledgments

This work used the Immersion GRating INfrared Spectrograph (IGRINS) that was developed under a collaboration between the University of Texas at Austin and the Korea Astronomy and Space Science Institute (KASI) with the financial support of the US National Science Foundation under grant AST-1229522, of the University of Texas at Austin, and of the Korean GMT Project of KASI. This research has made use of NASA's Astrophysics Data System Bibliographic Services, the HITRAN database operated by the Center for Astrophysics, and the SIMBAD database, operated at CDS, Strasbourg, France. This publication also makes use of data products from the Two Micron All Sky Survey, which is a joint project of the University of Massachusetts and the Infrared Processing and Analysis Center/California Institute of Technology, funded by the National Aeronautics and Space Administration and the National Science Foundation. Additionally, this work presents results from the European Space Agency (ESA) space mission Gaia. Gaia data are being processed by the Gaia Data Processing and Analysis Consortium (DPAC). Funding for the DPAC is provided by national institutions, in particular the institutions participating in the Gaia MultiLateral Agreement (MLA). Support from the Daniel Kirkwood Endowment at Indiana University is gratefully acknowledged. Finally, we thank the referee for their thoughtful comments that have materially improved our paper.

Facility: McDonald Observatory 2.7m Harlan J. Smith Telescope.

Software: IRAF (Tody 1986, 1993), MOOG (Sneden 1973, V. 2017), matplotlib (Hunter 2007), and numpy (van der Walt et al. 2011).

ORCID iDs

K. E. Brady https://orcid.org/0000-0003-3271-9434
C. Sneden https://orcid.org/0000-0002-3456-5929
C. A. Pilachowski https://orcid.org/0000-0002-3007-206X
Melike Afşar https://orcid.org/0000-0002-2516-1949
G. N. Mace https://orcid.org/0000-0001-7875-6391
D. T. Jaffe https://orcid.org/0000-0003-3577-3540
N. M. Gosnell https://orcid.org/0000-0002-8443-0723

References

Afşar, M., Sneden, C., Wood, M. P., et al. 2018, ApJ, 865, 44
Ahumada, J. A., & Lapasset, E. 2007, A&A, 463, 789
Allen, L. E., & Strom, K. M. 1995, AJ, 109, 1379
Amarsi, A. M., Barklem, P. S., Collet, R., et al. 2019, A&A, 624, A111
Angelo, M. S., Santos, J. F. C., Corradi, W. J. B., et al. 2019, A&A, 624, A8
Asplund, M., Grevesse, N., Sauval, A. J., et al. 2009, ARA&A, 47, 481
Bellini, A., Bedin, L. R., Piotto, G., et al. 2010, A&A, 513, A50
Bertelli Motta, C., Pasquali, A., Caffau, E., et al. 2018, MNRAS, 480, 4314
Charbonnel, C., & Lagarde, N. 2010, A&A, 522, A10
Cutri, R. M., Skrutskie, M. F., van Dyk, S., et al. 2003, yCat, II/246
de Mink, S. E., Langer, N., Izzard, R. G., et al. 2013, ApJ, 764, 166
Deng, L., Chen, R., Liu, X. S., et al. 1999, ApJ, 524, 824
Fabbian, D., Asplund, M., Carlsson, M., et al. 2006, A&A, 458, 899
Ferraro, F. R., Sabbi, E., Gratton, R., et al. 2006, ApJL, 647, L53
Gaia Collaboration, Brown, A. G. A., Vallenari, A., et al. 2018, A&A, 616, A1
Gao, X. 2018, ApJ, 869, 9
Gebran, M., Monier, R., Royer, F., et al. 2014, Putting A Stars into Context: Evolution, Environment, and Related Stars (Moscow: Pero), 193
Geller, A. M., Hurley, J. R., & Mathieu, R. D. 2013, AJ, 145, 8
Geller, A. M., Latham, D. W., & Mathieu, R. D. 2015, AJ, 150, 97
Gilliland, R. L., Brown, T. M., Duncan, D. K., et al. 1991, AJ, 101, 541
Girard, T. M., Grundy, W. M., Lopez, C. E., et al. 1989, AJ, 98, 227
González Hernández, J. I., & Bonifacio, P. 2009, A&A, 497, 497
Gustafsson, B., Edvardsson, B., Eriksson, K., et al. 2008, A&A, 486, 951
Hawkins, K., Masseron, T., Jofré, P., et al. 2016, A&A, 594, A43
Hills, J. G., & Day, C. A. 1976, ApJL, 17, 87
Hunter, J. D. 2007, CSE, 9, 90
Hurley, J. R., Pols, O. R., Aarseth, S. J., et al. 2005, MNRAS, 363, 293
Hurley, J. R., Tout, C. A., Aarseth, S. J., et al. 2001, MNRAS, 323, 630
Jacobson, H. R., Pilachowski, C. A., & Friel, E. D. 2011, AJ, 142, 59
Jadhav, V. V., Pandey, S., Subramaniam, A., et al. 2021, JApA, 42, 89
Jadhav, V. V., Sindhu, N., & Subramaniam, A. 2019, ApJ, 886, 13
Kippenhahn, R., & Weigert, A. 1967, ZAp, 65, 251
Landsman, W., Bohlin, R. C., Neff, S. G., et al. 1998, AJ, 116, 789
Latham, D. W., & Milone, A. A. E. 1996, The Origins, Evolution, and Destinies of Binary Stars in Clusters, 90, 385
Lauterborn, D. 1970, A&A, 7, 150
Lee, J.-J., & Gullikson, K. 2016, plp: v2.1 alpha 3 (v2.1-alpha.3), Zenodo. doi:10.5281/zenodo.560677
Leenaarts, J., Pereira, T. M. D., Carlsson, M., et al. 2013, ApJ, 772, 90
Leigh, N., & Sills, A. 2011, MNRAS, 410, 2370
Leiner, E., Mathieu, R. D., Gosnell, N. M., et al. 2018, ApJL, 869, L29
Leiner, E., Mathieu, R. D., Vanderburg, A., et al. 2019, ApJ, 881, 47
Leonard, P. J. T. 1996, ApJ, 470, 521
Liu, G. Q., Deng, L., Chávez, M., et al. 2008, MNRAS, 390, 665
Lombardi, J., Rasio, F. A., & Shapiro, S. L. 1995, ApJL, 445, L117
Lombardi, J. C., Warren, J. S., Rasio, F. A., et al. 2002, ApJ, 568, 939
Mace, G., Kim, H., Jaffe, D. T., et al. 2016, Proc. SPIE, 9908, 99080C
Mathys, G. 1991, A&A, 245, 467
Matrozis, E., Abate, C., & Stancliffe, R. J. 2017, A&A, 606, A137
McClure, R. D. 1997, PASP, 109, 536
McClure, R. D., & Woodsworth, A. W. 1990, ApJ, 352, 709
McCrea, W. H. 1964, MNRAS, 128, 147
Milone, A. A. E., & Latham, D. W. 1994, AJ, 108, 1828
Momany, Y., Held, E. V., Saviane, I., et al. 2007, A&A, 468, 973
Naoz, S., & Fabrycky, D. C. 2014, ApJ, 793, 137
Netopil, M., Paunzen, E., Heiter, U., & Soubiran, C. 2016, A&A, 585, A150
Nine, A. C., Mathieu, R. D., Gosnell, N. M., et al. 2023, ApJ, 944, 145
Packet, W. 1981, A&A, 102, 17
Pancino, E., Carrera, R., Rossetti, E., & Gallart, C. 2010, A&A, 511, A56
Pandey, S., Subramaniam, A., & Jadhav, V. V. 2021, MNRAS, 507, 2373
Park, C., Jaffe, D. T., Yuk, I.-S., et al. 2014, Proc. SPIE, 9147, 91471D
Park, S., Lee, J.-E., Kang, W., et al. 2018, ApJS, 238, 29
Perets, H. B., & Fabrycky, D. C. 2009, ApJ, 697, 1048
Pickles, A. J. 1998, PASP, 110, 863
Placco, V. M., Sneden, C., Roederer, I. U., et al. 2021, RNAAS, 5, 92
Preston, G. W., & Sneden, C. 2000, AJ, 120, 1014
Randich, S., Sestito, P., Primas, F., Pallavicini, R., & Pasquini, L. 2006, A&A, 450, 557
Sandage, A. R. 1953, AJ, 58, 61
Sanders, W. L. 1977, A&AS, 27, 89
Sandquist, E. L., Latham, D. W., Mathieu, R. D., et al. 2021, AJ, 161, 59
Sandquist, E. L., & Shetrone, M. D. 2003, AJ, 125, 2173
Santos, N. C., Lovis, C., Pace, G., Melendez, J., & Naef, D. 2009, A&A, 493, 309
Sarna, M. J., & De Greve, J.-P. 1996, QJRAS, 37, 11
Shetrone, M. D., & Sandquist, E. L. 2000, AJ, 120, 1913
Sills, A., Adams, T., & Davies, M. B. 2005, MNRAS, 358, 716
Sills, A., Faber, J. A., Lombardi, J. C., et al. 2001, ApJ, 548, 323
Sindhu, N. 2019, Ph.D Thesis, Vellore Institute of Technology
Sindhu, N., Subramaniam, A., & Radha, C. A. 2018, MNRAS, 481, 226
Sneden, C. 1973, ApJ, 184, 839
Soderblom, D. R., Stauffer, J. R., Hudon, J. D., et al. 1993, ApJS, 85, 315
Souto, D., Allende Prieto, C., Cunha, K., et al. 2019, ApJ, 874, 97
Stassun, K. G., van den Berg, M., Mathieu, R. D., et al. 2002, A&A, 382, 899
Stello, D., Vanderburg, A., Casagrande, L., et al. 2016, ApJ, 832, 133
Stryker, L. L. 1993, PASP, 105, 1081
Subramaniam, A., Pandey, S., Jadhav, V. V., et al. 2020, JApA, 41, 45

Tautvaišiene, G., Edvardsson, B., Tuominen, I., & Ilyin, I. 2000, A&A, 360, 499
Tody, D. 1986, Proc. SPIE, 627, 733
Tody, D. 1993, adass II, 52, 173
Tomkin, J., Lemke, M., Lambert, D. L., et al. 1992, AJ, 104, 1568
van den Berg, M., Tagliaferri, G., Belloni, T., et al. 2004, A&A, 418, 509
van der Walt, S., Colbert, S. C., & Varoquaux, G. 2011, CSE, 13, 22
Yong, D., Carney, B. W., & Teixera de Almeida, M. L. 2005, AJ, 130, 597
Yuk, I.-S., Jaffe, D. T., Barnes, S., et al. 2010, Proc. SPIE, 7735, 77351M